The apparent discontinuity in the periodicity of the GeV emission from LS I +61°303

F. Jaron, M. Massi
Max-Planck-Institute for Radio Astronomie, Auf dem Hügel 69, D-53121 Bonn, Germany

The γ-ray binary LS I +61°303 shows a discontinuity of the periodicity in its GeV emission. In this paper, we show that during the epochs when the timing analysis fails to determine the orbital periodicity, the periodicity is in fact present in the two orbital phase intervals $\Phi = 0.0 - 0.5$ and $\Phi = 0.5 - 1.0$. That is, there are two periodic signals, one towards periastron (i.e., $\Phi = 0.0 - 0.5$) and another one towards apastron ($\Phi = 0.5 - 1.0$). The apastron peak shows the same orbital shift as the radio outburst and, in addition, reveals the same two periods P_1 and P_2 that are present in the radio data. The γ-ray emission of the apastron peak normally just broadens the emission of the peak around periastron. Only when it appears at $\Phi = 0.8 - 1.0$ because of the orbital shift, it is detached enough from the first peak to become recognizable as a second orbital peak, which is the reason why the timing analysis fails. Two γ-ray peaks along the orbit are predicted by the two-peak accretion model for an eccentric orbit that was proposed by several authors for LS I +61°303.

1. Introduction

The stellar system LS I +61°303 is a member of the small class of γ-ray binaries, which are defined as binary stars with a peak in the spectral energy distribution above 1 MeV [1]. A sketch of the system is shown in Fig. 1. LS I +61°303 consists of a Be star and a compact object in an eccentric orbit, $e = 0.72 \pm 0.15$ [5], with orbital period $P_1 = 26.4960 \pm 0.0028$ d [6]. The Be star is rapidly rotating and losing mass in form of an equatorial disk [5]. The nature of the compact object could not yet be established, because the masses are poorly constrained due to the large uncertainty in the inclination angle [5]. The orbital phase of the binary system is defined as

$$\Phi = \frac{t - t_0}{P_1} - \mathrm{int}\left(\frac{t - t_0}{P_1}\right), \qquad (1)$$

where t_0 = MJD 43366.275 [6]. Periastron occurs at orbital phase $\Phi = 0.23$ [5].

Radio outbursts are observed at orbital phases $\Phi = 0.5 - 0.9$, i.e., around apastron. Their peak flux densities are modulated in amplitude and orbital phase occurrence by a long-term period $P_{\mathrm{long}} = 1667 \pm 8$ d [6]. The long-term phase Θ is defined analogous to the orbital phase Φ by replacing P_1 by P_{long}.

The source LS I +61°303 is highly variable and periodic all over the electromagnetic spectrum from radio to very high energy γ-rays [2, 5, 6, 7]. The GeV γ-ray light curve, as obtained using *Fermi* LAT data, has so far been reported to peak at orbital phases around periastron [2, 9] (see Fig. 1). Timing analysis shows that the orbital period is present in the *Fermi* LAT light curve from this source, however not with equal power all of the time [9, 10]. There are times (Θ-phases) when the period is outstanding and there are times when the period is completely absent from the power spectrum, as shown well in Fig. 4 of [10]. Moreover, Fig. 3 of [10] shows that GeV data also show the long-term periodical variation affecting the radio data, but only at a specific orbital phase interval, $\Phi = 0.5 - 1.0$, that is around apoastron.

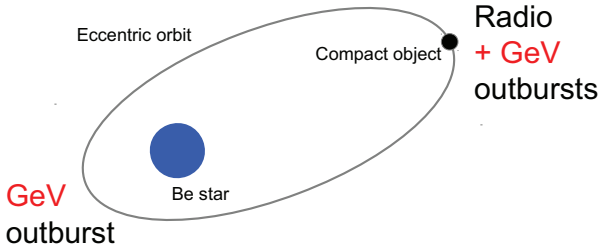

Figure 1: Sketch of LS I +61°303. The periodic GeV outburst at periastron was first reported by [2]. In Sect. 3 a newly discovered periodic apastron GeV peak is discussed [3]. The radio outburst occurs only at apastron, whereas at periastron, only a low level of emission is present [see Fig. 1-Right in 4].

We are aimed here to investigate the discontinuity in the periodicity of the GeV γ-ray emission at periastron, the possible relationship of its disappearance with the variation of the emission around apastron, and finally the possible relationship between GeV and radio emission.

2. Data analysis

For the present analysis [3] we use *Fermi* LAT data from LS I +61°303 spanning the time range August 5, 2008 (MJD 54683) until June 30, 2014 with an energy range of 100 MeV to 300 GeV. For the computation of the light curves we used

the script like_lc.pl written by Robin Corbet. [1] Only source-event-class photons were selected for the analysis. Photons with a zenith angle greater than 100° were excluded to reduce contamination from the Earth's limb. For the diffuse emission we used the model gll_iem_v05_rev1.fit and the template iso_source_v05_rev1.txt. We used the instrument response function (IRF) P7REP/background_rev1, and the model file was generated from the 2FGL catalogue [11], all sources within 10° of LS I +61°303 were included in the model. LS I +61°303 was fitted with a log-parabola spectral shape and with all parameters left free for the fit, performing an unbinned maximum likelihood analysis. The other sources were fixed to their catalogue values. We produced light curves with a time bin size of one day and of five days.

We investigated [for details see 3] the temporal evolution of the orbital periodicity by means of a wavelet analysis [12] and Lomb-Scargle timing analysis [13, 14].

3. Results: A periodic signal around apastron

3.1. Wavelet analysis

Our results are shown Fig. 2. The first plot of Fig. 2 presents the examined data set. The wavelet analysis was applied to the γ-ray data vs time, however, for a straightforward comparison with radio data, we express in the other plots of Fig. 2 the x-axis as the long-term phase Θ. The second plot of Fig. 2 shows the wavelet plot for the whole data set, i.e., the whole orbital period $\Phi = 0.0-1.0$. The absence of the orbital period around $\Theta \approx 7.2$ is consistent with the previous finding shown in Fig. 4 of [10]. When wavelet analysis is performed only on data from the orbital phase intervals $\Phi = 0.0 - 0.5$ (middle) and $\Phi = 0.5 - 1.0$ (bottom), it is revealed that *there is always a periodic signal at* $\Phi = 0.0-0.5$ *(periastron). Moreover, there is a periodic signal at* $\Phi = 0.5 - 1.0$ *(apastron).* The latter becomes particularly strong during the time when the orbital period is absent from the power spectra of $\Phi = 0.0 - 1.0$ [3].

3.2. Lomb-Scargle timing analysis

Figure 3 shows Lomb-Scargle periodograms of the γ-ray flux from LS I +61°303. The data have been selected from orbit phase intervals like in the previous section. In the periodogram for the entire orbit (Fig. 3 a) the strongest feature is a peak which agrees well with the orbital period P_1 found by [17]. Figures 3 d, e, and f, refer to only data from $\Phi = 0.5-1.0$. In this orbital phase interval the peak at $P_{\rm long}$ is a very strong feature, in agreement with the findings of [10]. Moreover, the zoom of Fig. 3 d, i.e., Fig. 3 e, shows a second peak, $P_2 = 26.99 \pm 0.08$ d. This second peak becomes stronger and is almost as strong as the peak at $P_1 = 26.48 \pm 0.08$ d in the 5 day integrated data in Fig. 3 f. The periods P_1, P_2 (see Fig. 4), and $P_{\rm long}$ here present are typical periodicities in radio data as shown in [15].

3.3. Folded *Fermi* LAT data: The apastron GeV peak and its orbital shift

Figure 5 a and b show *Fermi* LAT data from the time ($\Theta \approx 7.2$) of the disappearance of the orbital period from the power spectra folded with the orbital period. A second peak is evident at orbital phases $\Phi = 0.8 - 1.0$. Figure 5 c shows *Fermi* LAT data for another Θ. It is now interesting to compare these plots with radio data. Because of the long-term periodicity we can compare γ-ray and radio data having the same fractional part of Θ. Figure 5 d shows GBI radio data at 8 GHz [for details see 3].

4. Conclusions

During the intervals where the orbital periodicity is absent from the power spectra, wavelet and the folded light curves show two periodic signals, one at periastron and a second at apastron. The presence of the second periodic outburst disturbs the timing analysis and prevents it from finding the orbital periodicity. Comparison with the folded radio data (Fig. 4 d) suggests that the apastron GeV peak follows the same orbital shift as the radio outbursts [3]. It is well-known the phenomenon of the orbital shift of the radio outburst in LS I +61°303: The largest outbursts occur at orbital phase 0.6, afterwards, with the long-term periodicity, the orbital phase of the peak of the outburst changes, as analysed by [16] in terms of orbital phase shift, by [17] in terms of timing residuals, and reproduced recently by the precessing jet model in [18], here shown in Fig. 5.

Our result of two GeV peaks along the orbit corroborates the two-peak accretion model for LS I +61°303. The hypothesis that a compact object that accretes material along an eccentric orbit undergoes two accretion peaks along the orbit was suggested and developed by several authors for the system LS I +61°303 [19, 20, 21, 22]. The first accretion peak is predicted to occur close to the Be star and to give rise to a major high-energy outburst. The second accretion peak is predicted to occur much farther away from the Be star, where the radio outburst occurs, and a minor

[1] http://fermi.gsfc.nasa.gov/ssc/data/analysis/user/

high-energy outburst is predicted there [21]. The predicted periastron event corresponds well to the observed GeV peak towards periastron, the second predicted high-energy outburst, corresponds well to the here discussed apoastron peak.

Acknowledgments

We thank Bindu Rani for carefully reading the manuscript and for useful comments. We thank Robin Corbet for answering our questions concerning the computation of light curves. We thank Walter Alef and Alessandra Bertarini for their assistance with computation power. Wavelet software was provided by C. Torrence and G. Compo, and is available at URL: `http://atoc.colorado.edu/research/wavelets/`. The Green Bank Interferometer was operated by the National Radio Astronomy Observatory for the U.S. Naval Observatory and the Naval Research laboratory during the time period of these observations. This work has made use of public *Fermi* LAT data obtained from the High Energy Astrophysics Science Archive Research Center (HEASARC), provided by NASA Goddard Space Flight Center.

References

[1] Dubus, G. 2013, A&A Rev., 21, 64
[2] Abdo, A. A., Ackermann, M., Ajello, M., et al. 2009, ApJ, 701, L123
[3] Jaron, F., & Massi, M. 2014, A&A, 572, AA105
[4] Massi, M., Jaron, F., & Hovatta, T. 2015, arXiv:1502.00934
[5] Casares, J., Ribas, I., Paredes, J. M., Martí, J., & Allende Prieto, C. 2005, MNRAS, 360, 1105
[6] Gregory, P. C. 2002, ApJ, 575, 427
[7] Albert, J., Aliu, E., Anderhub, H., et al. 2009, ApJ, 693, 303
[8] Massi, M., Ros, E., & Zimmermann, L. 2012, A&A, 540, AA142
[9] Hadasch, D., Torres, D. F., Tanaka, T., et al. 2012, ApJ, 749, 54
[10] Ackermann, M., Ajello, M., Ballet, J., et al. 2013, ApJ, 773, LL35
[11] Nolan, P. L., Abdo, A. A., Ackermann, M., et al. 2012,
[12] Torrence, C. & Compo, G. P. "A Practical Guide to Wavelet Analysis", Bulletin of the American Meteorological Society, 1998, 61-78
[13] Lomb, N. R. 1976, Ap&SS, 39, 447
[14] Scargle, J. D. 1982, ApJ, 263, 835
[15] Massi, M., & Jaron, F. 2013, A&A, 554, AA105 ApJS, 199, 31
[16] Paredes, J. M., Estalella, R., & Rius, A. 1990, A&A, 232, 377
[17] Gregory, P. C., Peracaula, M., & Taylor, A. R. 1999, ApJ, 520, 376
[18] Massi, M., & Torricelli-Ciamponi, G. 2014, A&A, 564, AA23
[19] Taylor, A. R., Kenny, H. T., Spencer, R. E., & Tzioumis, A. 1992, ApJ, 395, 268
[20] Marti, J., & Paredes, J. M. 1995, A&A, 298, 151
[21] Bosch-Ramon, V., Paredes, J. M., Romero, G. E., & Ribó, M. 2006, A&A, 459, L25
[22] Romero, G. E., Okazaki, A. T., Orellana, M., & Owocki, S. P. 2007, A&A, 474, 15

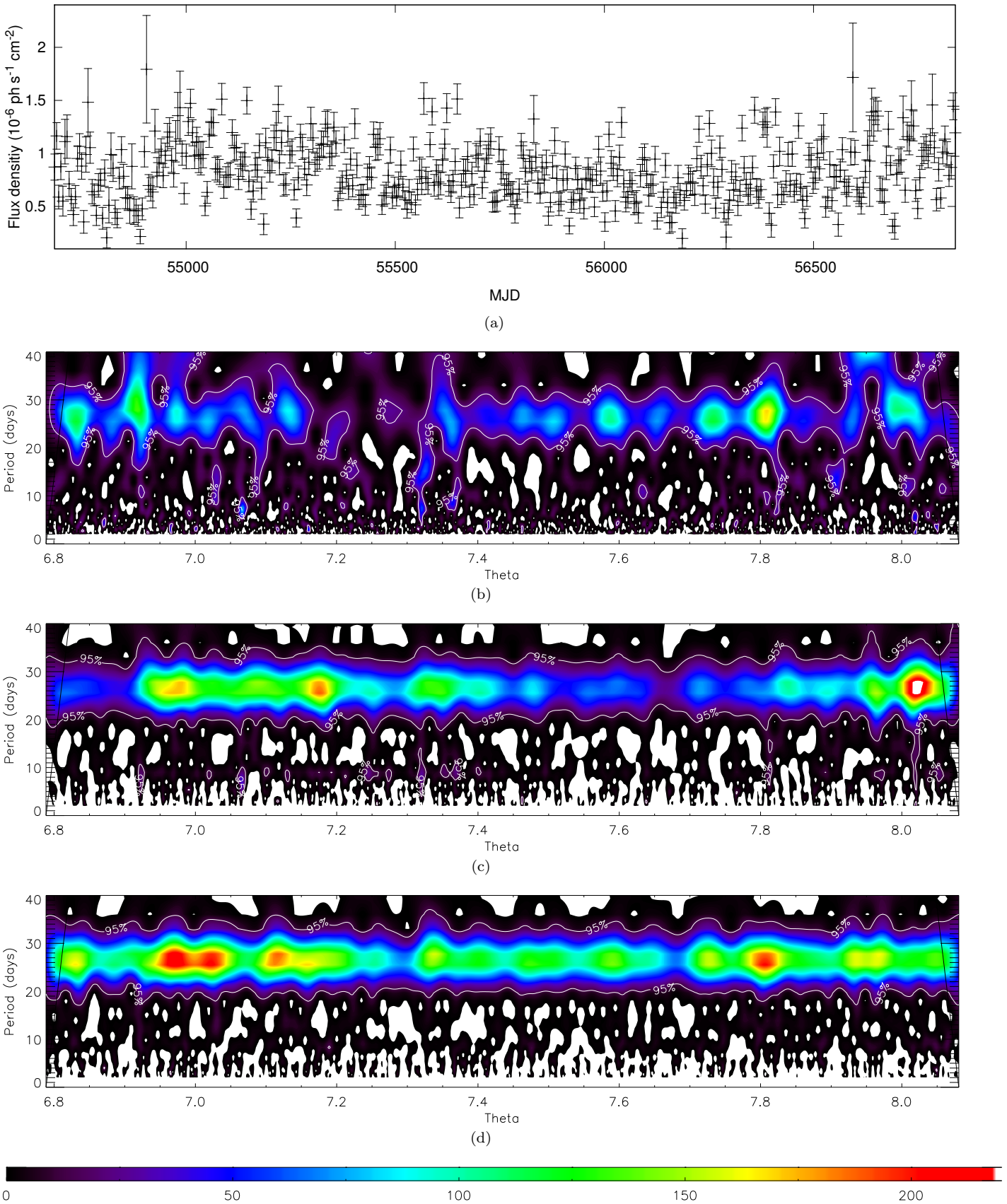

Figure 2: Wavelet analysis of *Fermi*-LAT data. The strength of periodicity is colour coded as indicated in the bottom bar. (a) *Fermi*-LAT data with a time bin of 1 d. (b) Wavelet analysis for the whole orbital interval $0.0 - 1.0$ (b–d use a time bin of one day). (c) Wavelet analysis for the orbital interval $\Phi = 0.5 - 1.0$, i.e., around apoastron. (d) Wavelet for the orbital interval $\Phi = 0.0 - 0.5$, i.e., around periastron.

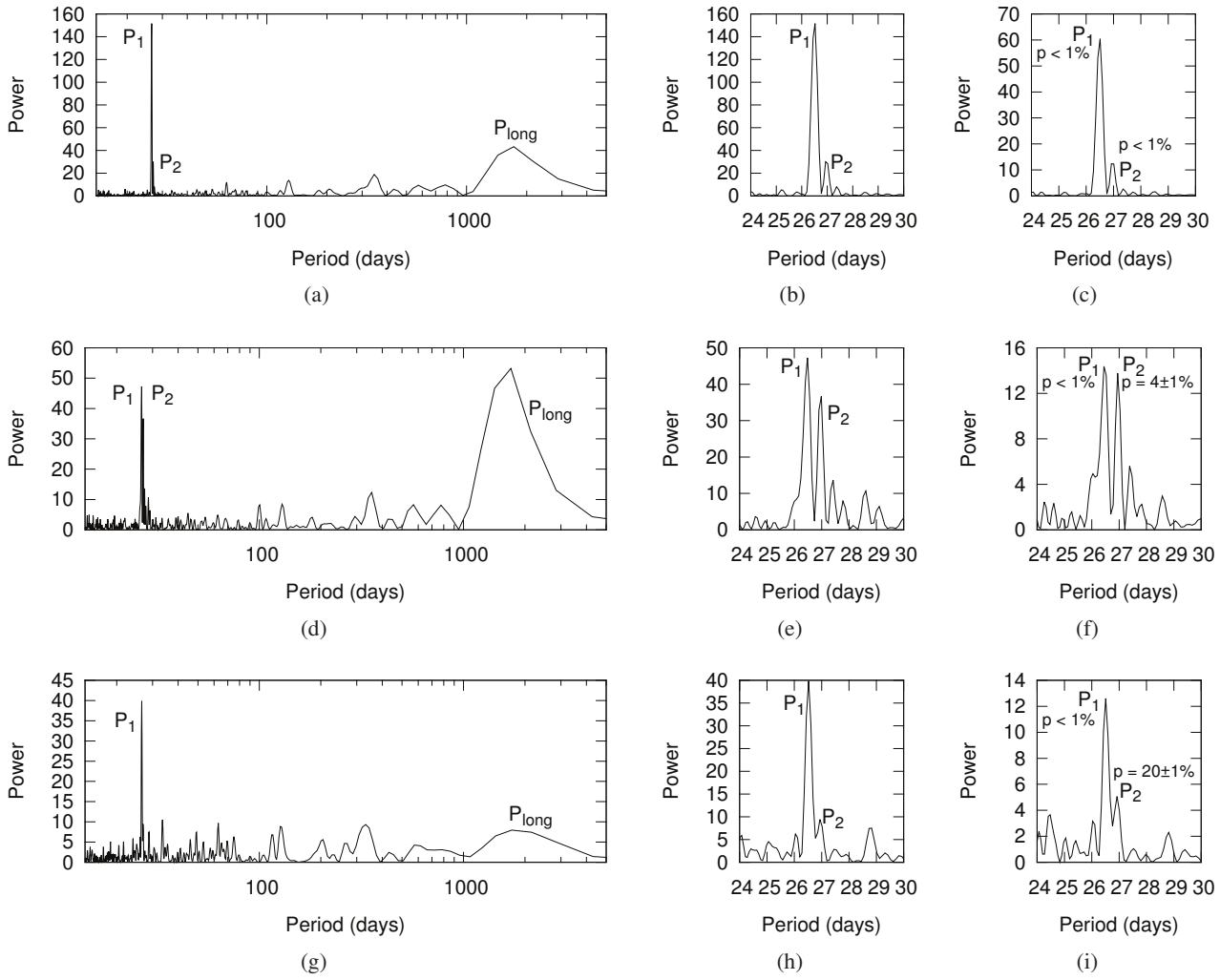

Figure 3: Lomb-Scargle periodogram of the *Fermi* LAT data (with a time bin of one day). Figure 3 in [3]. (a) Data in the orbital phase $\Phi = 0.0 - 1.0$. (b) Zoom of Fig. 3 a. (c) Same as 3 b for data with a time bin of 5 d. (d) Data in the orbital phase $\Phi = 0.5 - 1.0$. The periods P_2 and $P_{\rm long}$ here present are typical periodicities in radio data [15]. (e) Zoom of Fig. 3 d. (f) Same as 3 e for data with a time bin of 5 d. (g) Data in the orbital phase $\Phi = 0.0 - 0.5$. (h) Zoom of Fig. 3 g. (i) Same as 3 h for data with a time bin of 5 d.

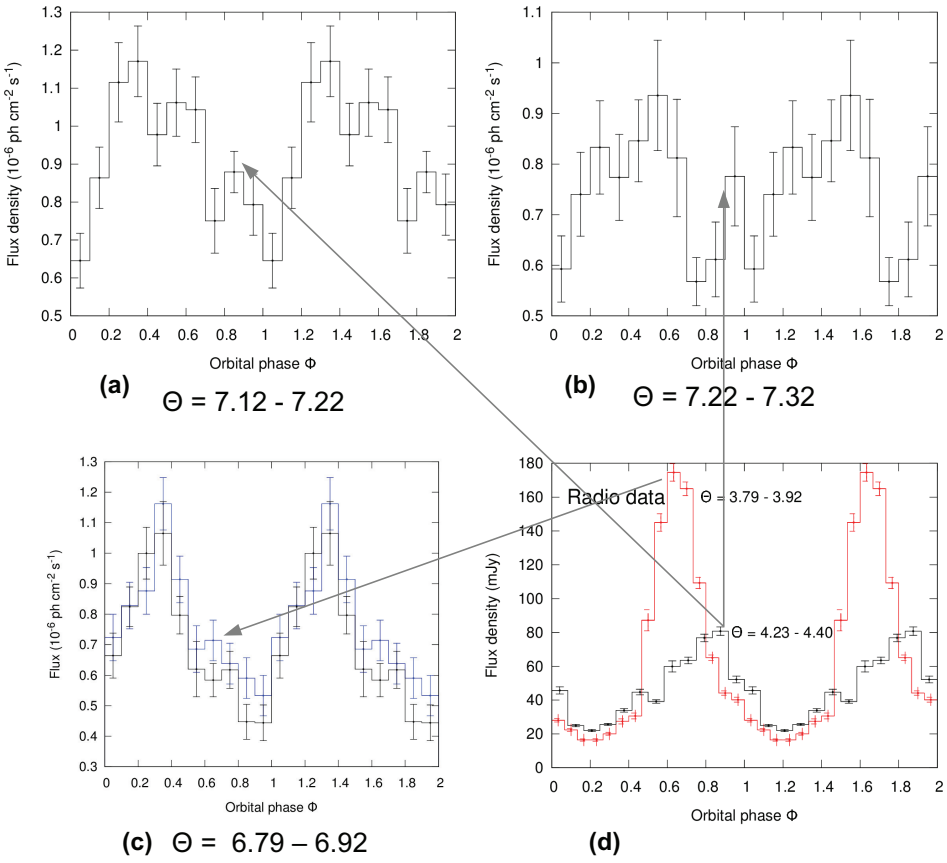

Figure 4: (a)-(c) Folded *Fermi* LAT γ-ray data (100 MeV – 300 GeV). The blue curve in (c) is that of [9]. (d) Folded GBI 8 GHz radio data. The here discovered periodic apastron GeV peak follows the same timing characteristic (i.e., P_1 and P_2 are both present) as the periodic radio peak, which also occurs around apastron. During the time when the orbital period disappears from the power spectra of the γ-ray light curve (see Fig. 2 b, $\Theta \approx 7.2$) the apastron GeV peak becomes well visible in the folded light curve, because it is more displaced from the periastron peak (see [3] and here Sect. 4).

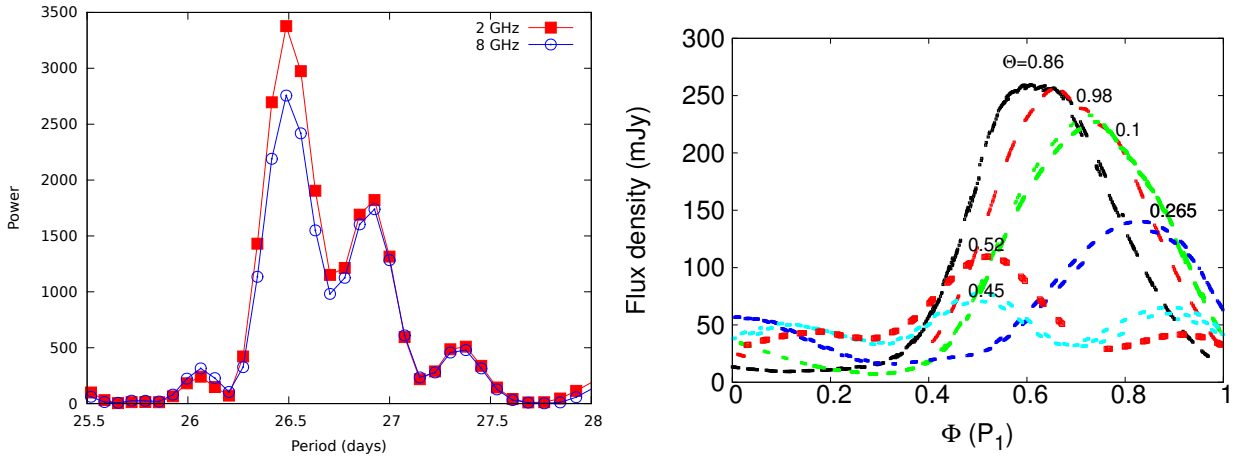

Figure 5: Left: Timing analysis of 6.7 years of GBI radio data at 2 and 8 GHz results in two periods, $P_1 = 26.49 \pm 0.07$ d, $P_2 = 26.92 \pm 0.07$ d. The long-term period $P_{\rm long} = 1667 \pm 8$ d is consistent with the period $P_{\rm beat} = 1/(\nu_1 - \nu_2) = 1667 \pm 393$ d resulting from the beating between the two close periodicities P_1 and P_2 [15]. Right: Orbital shift of the radio outburst of LS I +61°303 in the precessing jet model of [18]. At $\Theta = 0.86$ the outbursts peak at $\Phi \approx 0.6$. At $\Theta = 0.265$ the outbursts peak at $\Phi \approx 0.85$.